# A method of cloud field detection over Antarctica during the polar night using AVHRR data

Makoto Kuji[1], Nobuyuki Kikuchi[2], Naohiko Hirasawa[3]
and Takashi Yamanouchi[3]

[1] *Department of Information and Computer Sciences, Nara Women's University,
Kitauoya Nishimachi, Nara 630-8506*
[2] *Center for Atmospheric and Oceanic Studies, Graduate School of Science,
Tohoku University, Sendai 980-8578*
[3] *National Institute of Polar Research, Kaga 1-chome, Itabashi-ku, Tokyo 173-8515*

***Abstract:*** An improved algorithm for cloud field detection over the Antarctic region is presented. The algorithm is a combination of a conventional split window method and a spatial coherence method. The conventional split window method utilizes the brightness temperature and the brightness temperature difference between split window channels. The spatial coherence method makes use of the standard deviation of the brightness temperature difference between split window channels as an index of cloud field homogeneity. The algorithm, in principle, enables us to detect an inhomogeneous cloud field which has not been well detected with only the conventional split window method. This algorithm was applied to Advanced Very High Resolution Radiometer (AVHRR) data during the polar night over the Antarctic region. It is found that the improved algorithm seems to work well for an inhomogeneous cloud field as expected, although there still remains uncertainty related to the vertical structure of the cloud field. In order to investigate the vertical structure in detail, further analyses are needed such as comparison of the result to ground-based meteorological observation, radiative transfer simulation, and analysis of TIROS-N Operational Vertical Sounder (TOVS) data.

## 1. Introduction

Clouds play important roles in the earth climate system in terms of radiation budget as well as hydrological and energy circulation, resulting from their great variation in temporal and spatial domain. Consequently, it is useful to observe them extensively and frequently by satellite, such as the National Oceanic and Atmospheric Administration (NOAA) polar orbiter, over polar regions in particular. It is difficult, however, to distinguish clouds from the underlying surface of inland Antarctica because clouds and the underlying surface (snow and ice) have similar low temperature and high albedo.

Yamanouchi *et al.* (1987) developed a polar cloud detection algorithm which utilized the scatter diagram of brightness temperature and brightness temperature difference of split window channels (11 and 12 $\mu$m bands) of AVHRR. Based upon the algorithm, Murata and Yamanouchi (1997) studied the distribution of clouds over east Antarctica all through the year 1987 using AVHRR data. In the polar night, however,

cloud detection with a thermal infrared imager onboard a polar orbiter is difficult. Because of the very low temperature (around 180 K) of the targets such as cloud and surface (snow and ice), the AVHRR sensor suffers from noise due to limitation of the inherent sensor dynamic range (Yamanouchi et al., 1987). Consequently, ground-based observation supplementary to AVHRR analysis could improve the quality of cloud detection (Yamanouchi and Kawaguchi, 1992). Recently, Yamanouchi et al. (2000) further suggested that the temporal variation of brightness temperature of AVHRR channel 4 (11 μm band) enables us to detect cloud on which the conventional split window approach (Yamanouchi et al., 1987) does not work well.

It is also suggested that some kinds of cloud field are not detected at all with satellite remote sensing, resulting from ground observation in inland Antarctica during the polar night. Ground-based observation data such as upward- and downward-flux and air temperature indicate that there are three cloud types. The first type (type 1) is a homogeneous and transparent cloud layer well detected with the conventional cloud detection method. The second type (type 2) is an inhomogeneous or broken cloud field only recognized by eye observation in the polar night. Finally, the third type (type 3) is a "phantom" cloud, which is not detected either with the conventional method using satellite remote sensing or by eye from the ground, although ground-based upward- and downward-flux and radiosonde air temperature data indicate the presence of clouds.

In this study, an improved algorithm to detect an inhomogeneous cloud field (type 2) is presented. This algorithm is, in principle, based upon a combination of the conventional split window method (Yamanouchi et al., 1987) and the spatial coherence method (Coakley and Bretherton, 1982). This algorithm was applied to the NOAA-14/AVHRR data received at Syowa Station. The analyzed result is discussed, compared to a result with a conventional cloud detection method, and then possible interpretations given.

## 2. Data and analysis

In this study, thermal infrared (split window) channels are used, such as channel 4 (11 μm band) and channel 5 (12 μm band) of NOAA-14/AVHRR data. The data of channel 3 are, however, not used because they are insensitive to temperature at very low temperature (Yamanouchi et al., 1987). Figure 1 shows the channel 4 image of AVHRR data at 1345 UTC July 6, 1997, received at Syowa Station. The scene in Fig. 1, which includes Syowa Station, consists of 512 by 512 pixels resampled simply every 4 pixels in the along and cross track directions from the head portion of the original image. It can be seen in Fig. 1 that the lower temperature portion (more dense black region) corresponds to the ridge of the eastern part of the Antarctic ice sheet. There is what looks like a cloud system along the topography in the right portion of the image in Fig. 1.

Figure 2 shows the image of channel 4 brightness temperature analyzed in this study. The image contains 512 by 512 pixels cut out of the original image and is approximately equivalent to the 558 by 589 km$^2$ region. The image center is located at the 1536-th line and 1792-th scan (77.90°S and 14.17°E) which corresponds to upper left region of the image in Fig. 1. It can be seen in Fig. 2 that there existed a higher
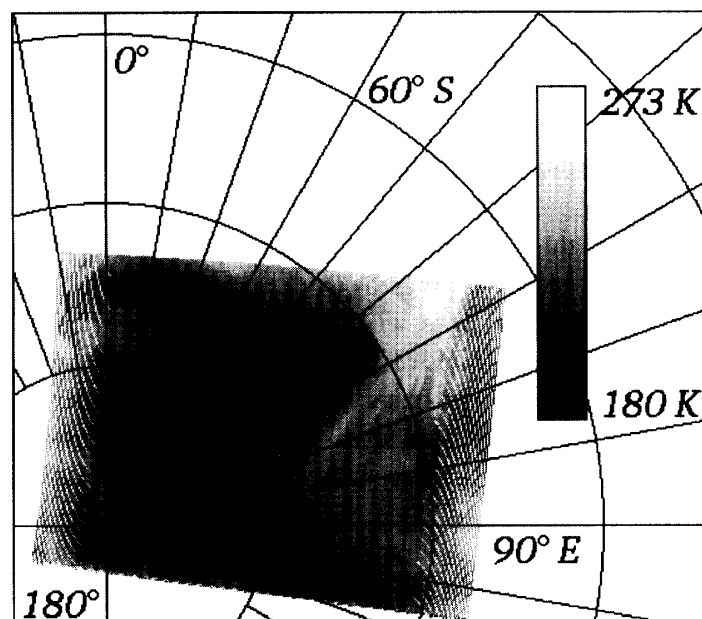
Fig. 1.   An example of channel 4 brightness temperature imagery of NOAA-14/AVHRR
data, archived in the National Institute of Polar Research.   These data were
received at Syowa Station (69°00'S, 39°35'E) on 1345 UTC July 6, 1997.   The
level slice is assigned as a gray scale linearly from 273 K (white) to 180 K
(black).   The image is projected as a polar stereo.   The South Pole is located in
the left bottom corner of the panel.   Latitudinal circle lines are drawn radially
every 10° from 90°S (South Pole) to 50°S (only 60°S is labeled explicitly).
Longitude lines are drawn clockwise every 10° from 0° to 90°E, to 180°, to 90°
W (the horizontal line from South Pole to the left edge of the panel), and to 0°
again.   The NOAA polar orbiter flew from bottom to top along the center line
(not explicitly illustrated) of the image.   White points scattered around the right
and left side of the image indicate data loss due to the 4 by 4 resampling; this
loss only affects the displayed image.   There is no problem in actual data
analysis as illustrated in Fig. 2.

temperature portion (more dense white region) which is believed to be a cloud system
due to the peculiar pattern.    It also appears that at the left half portion of the image in
Fig. 2, there is wrinkle structure in black and white corresponding to the surface ups and
downs.

The segment analysis adopted in this study is explained in Fig. 3.   The 512 by 512
pixels in Fig. 3a are equivalent to the image of Fig. 2.   Averaging 4 by 4 pixels in Fig.
3a leads to 128 by 128 spots (Fig. 3b).   And then, one unit is set as 4 by 4 spots (Fig.
3c), which results in 32 by 32 units so as to be used for a segment analysis.   This
segment analysis is fundamentally based upon the approach adopted by Yamanouchi et
al. (1987).   Since original AVHRR data with full resolution have discrete (or
digitized) values due to the Analog to Digital (AD) conversion process onboard NOAA
polar orbiter, it is supposed that the values of spots (averaged 4 by 4 pixels) reflect more
natural characteristics of the cloud fields than those of pixels themselves in full
resolution.   Here, the averaging size from pixels to a spot and the unit size are both 4
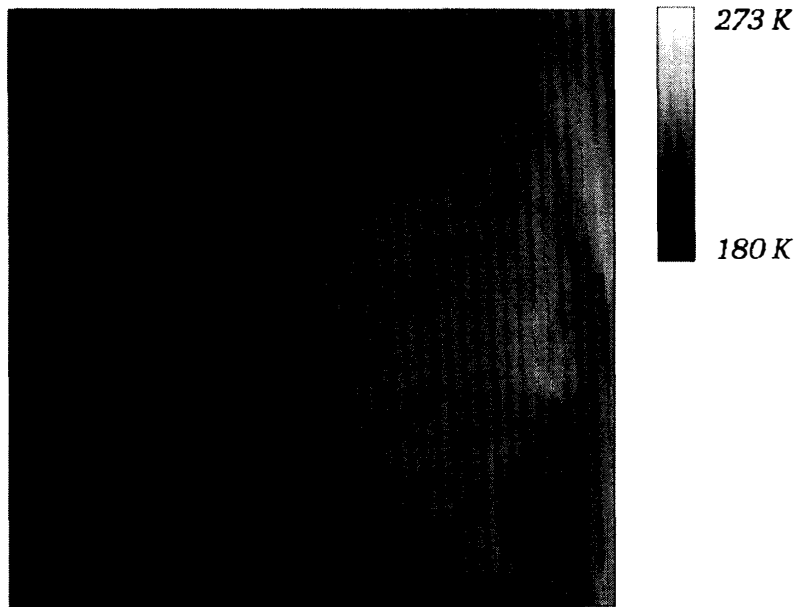
Fig. 2.   The same as Fig. 1, except for the image, which contains 512 by 512 pixels with full
          resolution cut out of the original image.   The image center is located at the intersection of
          the 1536-th line (along track) and 1792-th scan (cross track) which is in the upper left part
          of Fig. 1 (77.90°S, 14.17°E).   The level slice is assigned as a gray scale linearly from 273
          K (white) to 180 K (black).   The NOAA polar orbiter flew from top to bottom of the image.

### (a) Pixel                 (b) Spot                 (c) Unit

512 x 512 pixels         128 x 128 spots           32 x 32 units



                         * 1 spot:                  * 1 unit: 4 x 4 spots
                         4 x 4 pixels, averaged
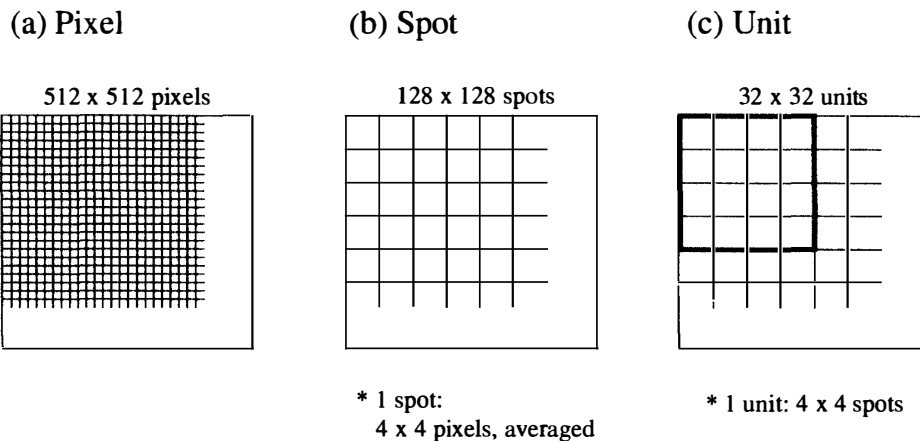
Fig. 3.   An explanation of the segment analysis: (a) original image in full resolution (512 by 512
          pixels), (b) spot image (128 by 128 spots) averaged over 4 by 4 pixels from the original
          image, and (c) unit image (32 by 32 spots) where each unit consists of 4 by 4 spots, used
          for the segment analysis adopted in this study.

by 4 (factor 4, i.e., $2^2$), which is conventional (Yamanouchi et al., 1987).   Additional
options were examined (not shown in this article) varying the unit size from $2^1$ to $2^5$ to
make units directly from pixels.   As a result, the unit analysis in this study showed
rather distinctive feature comprehensively in terms of cloud field detection than the

analysis with the units directly composed of factor $2^4$ basis.    Consequently, the conventional segment approach was adopted in this study again.

## 3.    Results and discussion

In this section, the results of the segment analysis based upon the conventional cloud detection method and the spatial coherence method are shown so as to discuss the possibility of inhomogeneous cloud field detection.

### 3.1.    Conventional cloud detection method and spatial coherence approach

A scatter diagram is shown in Fig. 4.    It results from the conventional split window cloud detection method (Yamanouchi et al., 1987) being applied to 32 by 32 units, as illustrated in Fig. 3c.    Figure 4 indicates that three major clusters exists in the scene (Fig. 2): (1) a cluster which is distributed around the mean value of the difference of brightness temperature with 0 K and is probably a clear sky region; (2) a cluster corresponding to one leg of an arch structure above the previous clear sky cluster, which is assumed to consist of high level clouds; and (3) a cluster which is distributed below the previous clear sky cluster and is believed to be low level clouds related to a surface temperature inversion.    The simultaneous appearance of clusters of case 2 (high level clouds) and case 3 (low level clouds with surface temperature inversion) is a characteristic feature of the inland region during the polar night.    The reason for these inferences is that, in case 2, the temperature of the cloud layer is lower than that of the surface, vice versa in case 3 (Yamanouchi et al., 1987).    As easily seen from Fig. 4, it is not
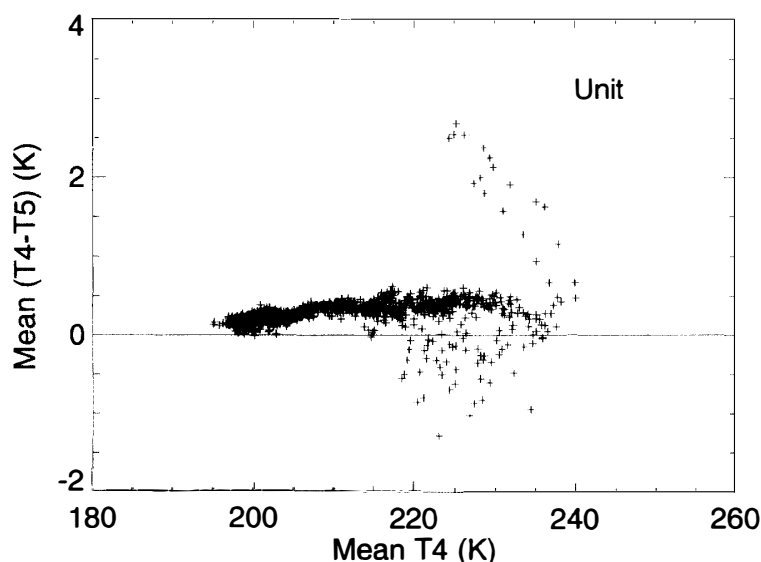


Fig. 4.    A scatter plot after the conventional cloud detection algorithm was applied to the segment data set (each unit), inland Antarctica, during the polar night.    This figure shows the relationship between the unit mean values of the brightness temperature difference $T_4$–$T_5$ (ordinate) and the unit mean values of the brightness temperature of channel 4 $T_4$ (abscissa).    The line where the unit mean value of the brightness temperature difference is equal to 0K is overlaid as a reference.
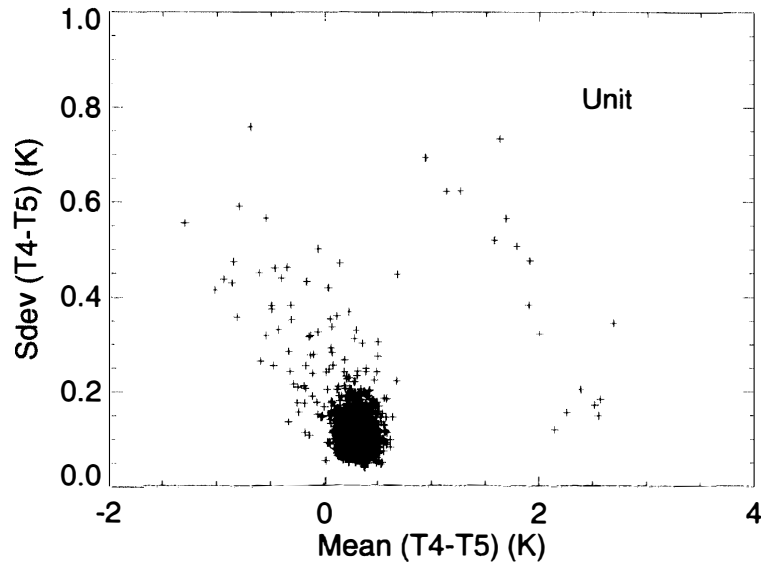
Fig. 5. As in Fig. 4, except that this figure shows the relationship between the unit standard deviation values of the brightness temperature difference $T_4$-$T_5$ (ordinate) and the unit mean values of the brightness temperature difference $T_4$-$T_5$ (abscissa).

straightforward to distinguish clusters from each other using only the mean value of the difference of brightness temperature in a unit. Consequently, Murata and Yamanouchi (1997), for example, classified clouds against surface with the correlation coefficient of each cluster as an additional parameter.

In this study, a scatter diagram between standard deviation and mean of the brightness temperature difference for each unit is also used to distinguish the three clusters from each other, as illustrated in Fig. 5. In Fig. 5, it is expected that in case of the smaller standard deviation values of the brightness temperature difference $T_4$-$T_5$, there are more spots filled with homogeneous features, while in case of the larger standard deviation values, on the other hand, there are more spots filled with inhomogeneous features in the units. For example, the cluster of case 1 (clear sky region) in Fig. 4 is distributed densely around the mean value 0.25 K and standard deviation value 0.125 K in Fig. 5; the cluster of case 3 in Fig. 4, on the other hand, is distributed continuously from the cluster of case 1 to the portion of the larger standard deviation values. This indicates that the lower level cloud region inhomogeneously extends over the clear sky region in each unit. For the cluster of case 2 (high level clouds), there are some units which have rather small standard deviation values (less than about 0.2 K), which indicates that a high level cloud layer homogeneously extends across the units.

### 3.2. Schematic diagram

Figure 6 schematically illustrates an ideal situation which is possible to explain Figs. 4 and 5. Supposing that there are just three major components over the field observed with AVHRR such as surface with clear sky condition, transparent (homogenous) high level cloud layer, and transparent (homogenous) low level cloud layer at the inversion layer with the profile illustrated in Fig. 6a, then the spatial coherence diagram

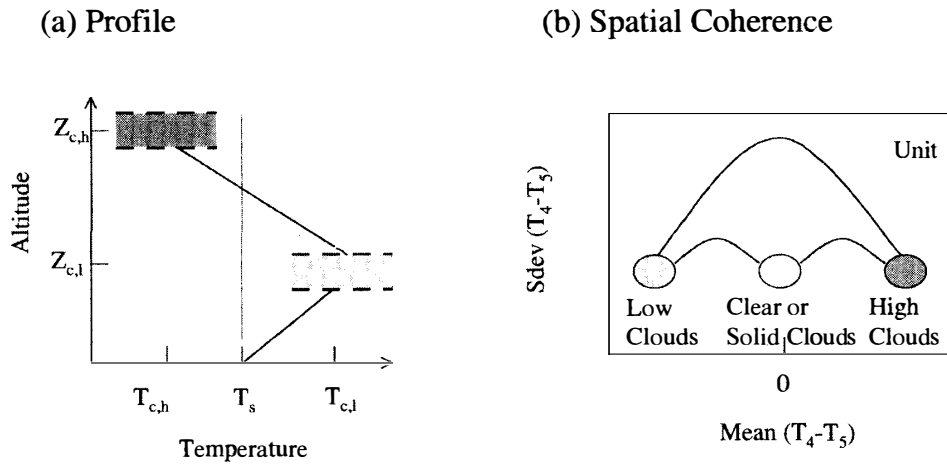(a) Profile                          (b) Spatial Coherence



Fig. 6.   A schematic diagram of an ideal case of a cloud field and the underlying surface for interpretation of Figs. 4 and 5.   (a) temperature profile with cloud layers: one layer is at high level and the other is at low level around surface temperature inversion, where $T_s$ is surface temperature $T_{c,h}$ is high level cloud temperature at the level $Z_{c,h}$, and $T_{c,l}$ is low level cloud temperature at the level $Z_{c,l}$.   (b) spatial coherence relationship between standard deviation and mean values for the brightness temperature difference $T_4-T_5$ in the units for the ideal case illustrated in panel (a).

in Fig. 6b applies.

In Fig. 6b, there are three dense clusters (so-called 'super' clusters referred to in Coakley and Bretherton, 1982) in the parts of smaller standard deviation values of $T_4$–$T_5$ for each component, corresponding to three mean values of $T_4$–$T_5$ such as positive, around zero, and negative, respectively.   And then, if there are now just two components such as transparent high level cloud and surface, the scatter plot is expected to be distributed along the arch between those two components (super clusters) on the analogy of the spatial coherence diagram for the brightness temperature $T_4$ (Coakley and Bretherton, 1982).   The larger standard deviation value portion (leg of an arch) indicates that the target region consists of a mixture of two components, that is, the field seems inhomogeneous in terms of $T_4$–$T_5$.   Consequently, in case of the three components mentioned above, it is anticipated that scatter plots will be distributed within the three envelope lines.

From Fig. 4, it is inferred that there are three clusters such as a clear sky field (case 1), high level cloud layer (case 2), and low level cloud field (case 3).   And now from Fig. 5, it turns out that the high level clouds (case 2) have a homogeneous portion (type 1) with smaller standard deviation, while low level clouds (case 3), on the other hand, may be inhomogeneous (consisting of a rather broken field) which might be classified as type 2.   There are also other scatter plots distributed with larger standard deviation values and positive mean values within the three envelope lines illustrated in Fig. 6b, which suggests that these plots are expected to correspond to the multilayered system with high and low level clouds over surface.

Since Fig. 6b is a spatial coherence diagram in terms of $T_4$–$T_5$, not for brightness temperature $T_4$ itself, this kind of diagram also contains information about vertical

inhomogeneity such as cloud altitude, cloud geometrical thickness, and so on, as well as about horizontal inhomogeneity, optical and microphysical variability.   In this study, such speculation is critical because only two channel thermal infrared data are available under the condition of the polar night.   Data such as TOVS, with several channels sensitive to temperature of atmospheric vertical levels, are expected to enable us to investigate the multilayered cloud field in future.

### 3.3. Results of the combined method

Based upon the above discussion of Figs. 4, 5, and 6, at this stage, the following are expected: the AVHRR data over Antarctica during the polar night are classified into three cases: clear sky (ground), high level cloud, and low level cloud with the conventional cloud detection method (Yamanouchi et al., 1987).   Combined with the spatial coherence method (Coakley and Bretherton, 1982), the clear sky region has small standard deviation values of the brightness temperature difference, while the high and low level cloud fields can have large standard deviation values.   In this subsection, this will be illustrated with images.

Figure 7 gives the results of the segment analyses: (a) the mean of the brightness temperature of channel 4 $T_4$, (b) the mean of the difference of the brightness temperatures between channels 4 and 5 $T_4-T_5$, and (c) the standard deviation of $T_4-T_5$.   The whiter portion distributed around the right half of Fig. 7a corresponds to the portion of


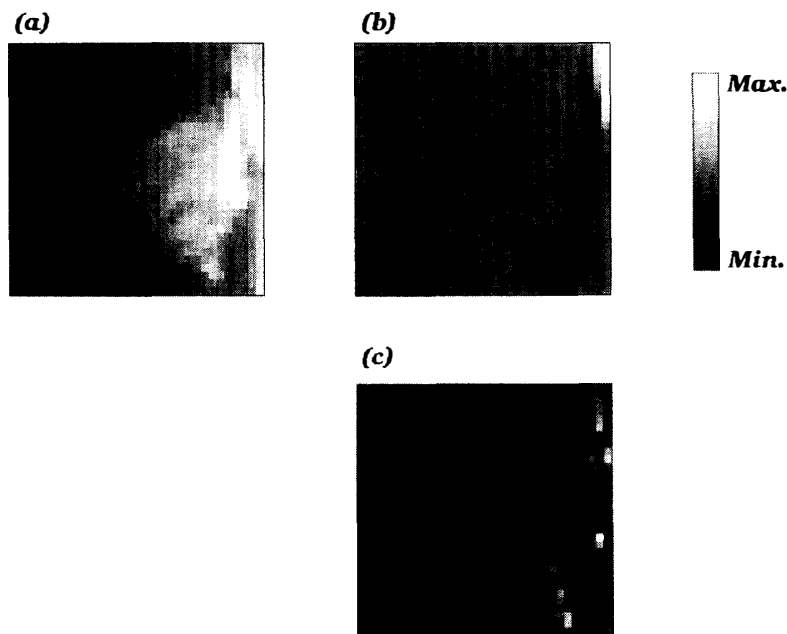
Fig. 7.   Maps of the results of the segment analyses: (a) the unit mean values of the brightness temperature of channel 4 $T_4$, (b) the unit mean values of the brightness temperature difference $T_4-T_5$, and (c) the unit standard deviation values of the brightness temperature difference $T_4-T_5$.   The level slice is assigned as a gray scale linearly from the maximum value (white) to the minimum value (black) for each panel.   Each panel consists of 32 by 32 units.   The NOAA polar orbiter flew from top to bottom of this figure, as in Fig. 2.

the larger $T_4$ in Fig. 4.    From Fig. 4, it is shown that there are three components: high level cloud, clear sky (ground), and low level cloud field, which also appear in Fig. 7b as whiter, gray, and blacker portions, respectively.

Portions corresponding to the low level cloud fields at right-middle to -bottom in Fig. 7b are whiter in Fig. 7c, and those cloud fields seem rather inhomogeneous.    This suggests that the standard deviation of $T_4$-$T_5$ is useful to detect an inhomogeneous cloud field as expected.    In Fig. 5, this inhomogeneous cloud field corresponds to the portion distributed continuously around negative Mean ($T_4$-$T_5$) and larger Sdev ($T_4$-$T_5$).    This inhomogeneous cloud field also corresponds to the portion enveloped between a so-called arch structure (cloudy region) and a base line (clear region) in the conventional diagram in Fig. 4, although in this case, the arch structure for low level cloud does not appear clearly.

The portion corresponding to the high level cloud field at the right-top in Fig. 7b is blacker in Fig. 7c, and the cloud field seems more homogeneous.    In Fig. 5, this homogeneous cloud field corresponds to the portion around the largest Mean ($T_4$-$T_5$) and smaller Sdev ($T_4$-$T_5$).    There is another, whiter, portion in Fig. 7c in the transition region from the inhomogeneous low level cloud fields to the homogeneous high level cloud field, which indicates the existence of a multilayered cloud system which consists of both components.    In Fig. 5, this transition region is distributed continuously from the portion around the largest Mean ($T_4$-$T_5$) and smaller Sdev ($T_4$-$T_5$) to the one with intermediate Mean ($T_4$-$T_5$) and larger Sdev ($T_4$-$T_5$).

The central portion in Fig. 7a seems to be a cloud field, judging from its peculiar pattern.    But in Fig. 7b, the pattern disappears because the difference of the brightness temperatures between cloud layer and surface becomes very small within the resolution of the dynamic range.    In Fig. 4, this portion corresponds to the right half of the cluster previously judged as a clear sky region (case 1), then it turns out that this portion is classified wrongly.    In Fig. 7c, further, the relevant central portions have a small enough standard deviation to be considered a homogeneous region.    Consequently, the cloud field, due to the small difference of brightness temperatures between cloud layer and surface, is not still detected well even after this additional spatial coherence analysis. This might be a case of a phantom cloud field (type 3).

## 4.  Concluding remarks

In order to study cloud variation over the Antarctic region using remote sensing data, NOAA-14 data received at Syowa Station were analyzed.    In this study, as a first step, an improved algorithm was developed to detect inhomogeneous cloud fields in inland Antarctica during the polar night, since this kind of field has not been interpreted clearly only with the conventional split window method.    This algorithm was applied to the NOAA-14/AVHRR data on 1345 UTC July 6, 1997.    As a result, it turned out that the algorithm successfully detected the inhomogeneous cloud field (type 2) as well as the homogeneous cloud (type 1) and clear sky region in combination with the conventional split window method.    It was found that the algorithm was not applicable to detecting some kinds of cloud, such as the so-called "phantom cloud" (type 3).    Concerning this phantom cloud (type 3), in situ active remote sensing observation with lidar has been

carried out by ground observers (*e.g.*, Hayashi, 1999) so as to determine cloud heights, which would be expected to resolve the uncertainty relevant to this type of cloud.

Due to the limitation of data to just two channels from AVHRR during the polar night in inland Antarctica, the analyzed results at present indicate that there exist horizontally inhomogeneous clouds or possibly a multilayered cloud system. Further work on the multilayered cloud system is encouraged. Such work could include i) comparison of the remote sensing result with ground observations, ii) numerical simulation with a radiative transfer model, and iii) data analysis of TOVS which observed simultaneously with the AVHRR onboard the same NOAA-14 polar orbiter.

## Acknowledgments

### References

Coakley, J.A., Jr. and Bretherton, F.P. (1982): Cloud cover from high-resolution scanner data: Detecting and allowing for partially filled fields of view. J. Geophys. Res., **87**, 4917–4932.

Hayashi, M. (1999): On observation of aerosol and atmospheric minor constituents at Dome Fuji Station. Tenki, **46**, 153–156 (in Japanese).

Murata, A. and Yamanouchi, T. (1997): Distribution characteristics of clouds over East Antarctica in 1987 obtained from AVHRR. J. Meteorol. Soc. Jpn., **75**, 81–93.

Yamanouchi, T. and Kawaguchi, S. (1992): Cloud distribution in the Antarctic from AVHRR data and radiation measurements at the surface. Int. J. Remote Sensing, **13**, 111–127.

Yamanouchi, T., Suzuki, K. and Kawaguchi, S. (1987): Detection of clouds in Antarctica from infrared multispectral data of AVHRR. J. Meteorol. Soc. Jpn., **65**, 949–962.

Yamanouchi, T., Hirasawa, N., Kadosaki, G. and Hayashi, M. (2000): Evaluation of AVHRR cloud detection at Dome Fuji Station, Antarctica. Polar Meteorol. Glaciol., **14**, 110–116.